Single-station vehicle tracking using six-component seismic measurements: A comparative study with array-based methods

Shihao Yuan*[1], Felix Bernauer[2], Joachim Wassermann[2], Eileen R. Martin[1,3], and Heiner Igel[2]

[1]Department of Geophysics, Colorado School of Mines, Golden, USA.

[2]Department of Earth and Environment Sciences, Ludwig-Maximilians-Universität München, Munich, Germany.

[3]Department of Applied Math and Statistics, Colorado School of Mines, Golden, USA.

October 14, 2024

Key words: Rotational ground motions, Direction of arrival (DOA), Bearing estimation, Source tracking, Rotational sensors, Ring laser gyroscopes, Fiber optic gyroscopes, Six-component (6C) measurement, Polarization analysis

*E-mail: syuan@mines.edu

Abstract

This study investigates the use of six-component (6C) seismic measurements for tracking moving traffic sources. We employ a collocated seismometer and rotational sensor to simultaneously capture both translational and rotational ground motions induced by vehicle sources. Our research demonstrates a novel method for determining source directionality using a single 6C station. This station has a small footprint, but it also allows us to extract directional information from both Rayleigh and Love waves. To validate our approach, we compare the estimated source directionality obtained from two different types of rotational sensors. Additionally, we compare our results against those derived from conventional array methods, including frequency-wavenumber analysis and array-derived rotation from a traditional seismic array deployed alongside our 6C stations. Our findings confirm the efficacy of the proposed 6C method in accurately locating vehicle sources. Importantly, the proposed 6C single-station measurement offers advantages over traditional array-based methods, particularly in environments where deploying multiple sensors is challenging. The success of this technique in traffic monitoring underscores its potential for broader applications, including real-time seismic source monitoring and early warning systems for geohazards. This study thus presents a significant advancement in seismic source tracking methodology, offering new possibilities for both urban and environmental seismic noise analysis.

Plain Language Summary

Knowing the direction of incoming seismic waves is essential for various studies, such as locating nuclear explosions, monitoring avalanches and landslides, and surveillance. Traditionally, this has been done using beamforming techniques, which require deploying seismic arrays with specific designs. However, these array-based methods can be difficult and impractical to deploy in environments like populated urban areas, ocean floors, mountains, and other planets. In this study, we present a new approach: using a single-station six-component (6C) measurement to estimate the direction of seismic sources. We apply this 6C technique to track moving vehicles and validate our findings against traditional array methods. Our results indicate that the 6C method is promising for real-time source monitoring.

1 Introduction

Seismic-based direction estimation is gaining increasing interest in surveillance systems because of the broadband sensitivities of seismic sensors. These sensors can detect not only natural events like earthquakes and landslides but also various anthropogenic ground motions, including human and vehicle movements. Recent studies have shown the effectiveness of seismic-based direction estimation across various fields. Avalanche monitoring using seismic sensors have been developed and proven effective at various sites over the past few decades (Almendros et al., 1999; Heck et al., 2019). Riahi and Gerstoft (2015) used an array of geophones to analyze traffic-related signals, demonstrating the usefulness of seismic data for traffic monitoring. Manconi et al. (2016) proposed a real-time method to detect and locate rockslides using seismic records. Additionally, Venkatraman et al. (2011) investigated seismic signals from moving heavy military vehicles to track their movements. Seismic data collected from dense networks has also been used to monitor the evolution of meteorological events, such as rainfall and thunderstorms, with unprecedented detail (Diaz et al., 2023).

The range of applications extends into fields like astrophysics and biology. For instance, Tape et al. (2020) employed seismometers to monitor auroras, while Reinwald et al. (2021) successfully located elephants using seismic sensors, offering new insights into their social interactions. In addition to traditional seismic instruments, more recent technologies like distributed acoustic sensing (DAS) have also been applied for seismic-based direction estimations. Martin et al. (2016) analyzed signals recorded by DAS along highways to locate sources of traffic noise, and Liu et al. (2019) developed a system for vehicle detection and classification using the same DAS technology.

Determining the source directionality of incoming seismic waves is typically achieved through methods such as beamforming or frequency-wavenumber (f-k) analysis (e.g., Krim and Viberg, 1996; Gal and Reading, 2019). These techniques extract coherent seismic energy that propagates to a seismic array based on trial slowness models. Alternatively, polarization analysis can be performed using a single triaxial seismic station, which is effective when pure modes of vibration are present (Greenhalgh et al., 2018).

Seismic sensors offer advantages over video or acoustic monitoring systems, as they are less affected by adverse weather conditions or environmental interference (Wang et al., 2014). However, when seismic stations are located very close to surface sources, Rayleigh and Love waves reach these stations almost simultaneously, leading to significant overlap in both the frequency and time domains. This overlap complicates the distinction between these wave types, making it challenging to apply existing techniques for estimating source directionality (Asgari et al., 2015). Additionally, the deployment and maintenance of seismic arrays can be costly. DAS technology provides a more economical alternative, especially when existing fiber-optic cables are used (Lindsey and Martin, 2021). However, its directional sensitivity may limit its ability to detect sources from multiple azimuths. Each of these methods has its strengths and limitations, highlighting the continued need for new methods to seismic source detection and localization.

In this study, we present an alternative approach for real-time seismic monitoring: a six-component (6C) single-station measurement that simultaneously captures both translational and rotational ground motions. We apply this method to track source directionality. First, we describe the seismic acquisition setup and source distributions at the Geophysical Observatory Fürstenfeldbruck in Germany. Next, we classify signals based on their temporal and spectral characteristics. We then demonstrate how to track moving vehicle sources using the 6C single-station measurement.

To validate our results, we cross-check the estimated source directionality using two types of rotational seismometers: a ring-laser gyroscope and a fiber-optic gyroscope. Additionally, we compare our findings with array measurements obtained through frequency-wavenumber (f-k) analysis and array-derived rotation (ADR). Finally, we discuss the advantages and limitations of the 6C single-station measurement. Throughout the study, we highlight the potential applications of this method for tracking various seismic and natural sources, especially in scenarios where deploying a seismic array is impractical.

2 Data acquisition

In combination with a classic broadband seismometer, the newly built ring laser gyroscope (named as ROMY) at the Geophysical Observatory Fürstenfeldbruck near Munich, Germany, allows us to record highly accurate and broadband 6C ground motions, i.e., 3C translational and 3C rotational motions, satisfying geodetic and seismic observations at various scales (Gebauer et al., 2020; Igel et al., 2021) (Figure 1). ROMY is a tetrahedral-shaped four-component rotational sensor (one auxiliary vertical component aligning on the horizontal surface) with each triangular side being approximately 12 m. FUR is a permanent station, belonging to the German Regional Seismic Network, equipped with a Streckeisen STS-2 sensor and a REFTEK RT130 datalogger. FUR and ROMY are just a few meters away from each other and thus are treated as one 6C single-station station. TON and FFB2–3, also serving as permanent stations, are particularly chosen to identify train- and car-related seismic signals considering their relative locations to the railway and highway nearby (blue and green curves shown in Figure 1). A small seismic array (DROMY and DRMY1–6), consisting of seven broadband sensors (Trillium compact 120s), are temporally deployed for the verification of the proposed 6C single-station measurement through f-k analysis. In addition to the ROMY ring laser gyroscope, we used a 6C measurement at Station BS that includes a collocated broadband seismometer and a portable rotational sensor. The rotational sensor, a fiber optic gyroscope (blueSeis-3A (Yuan et al., 2020b)), serves to cross-validate the moving vehicle monitoring for the 6C method alongside the ring laser gyroscope.

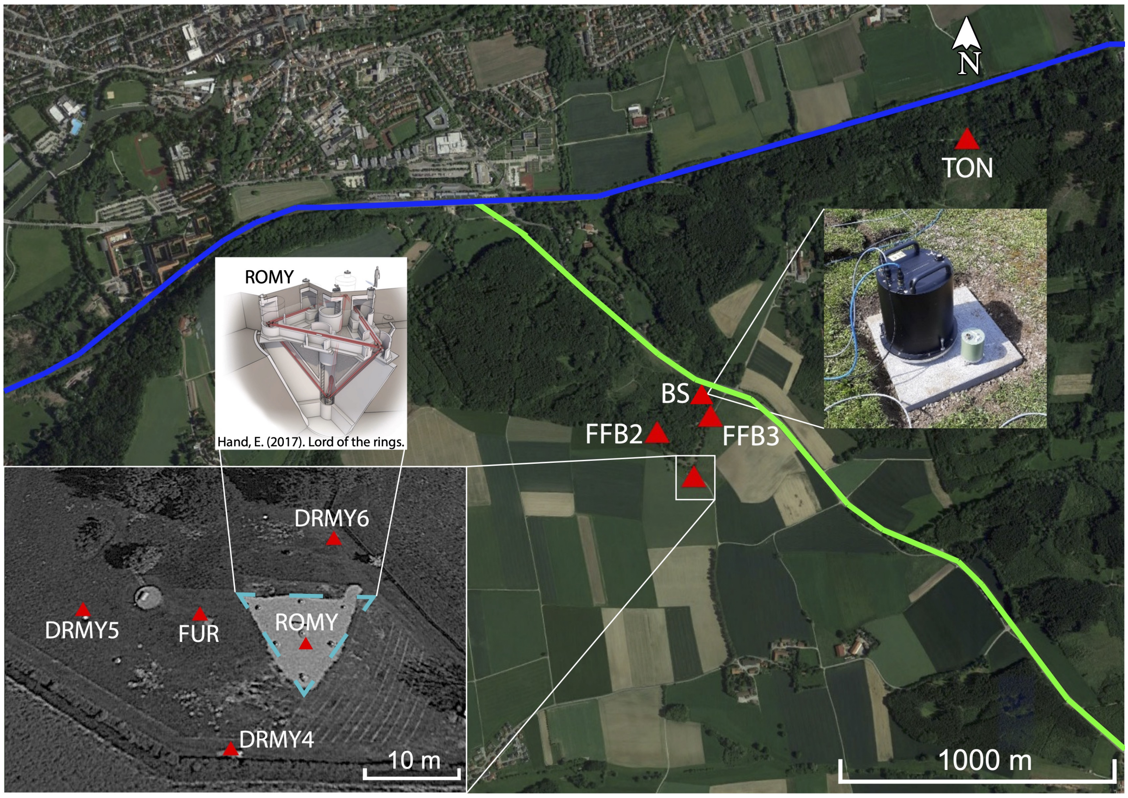

Figure 1: The site map and acquisition geometry at the Geophysical Observatory Fürstenfeldbruck, Germany, are shown here. Red triangles represent seismic stations. The bottom-left zoomed-in plots highlight the position of the 6C station (FUR+ROMY, with ROMY indicated by the blue dashed triangle) and the inner array (DROMY and DRMY1–6) used for frequency-wavenumber (f-k) analysis alongside stations FFB2–3. The upper-right zoomed-in plot displays the other 6C station, equipped with the collocated seismometer (grey) and the blueSeis-3A rotational sensor (black). Aside from ROMY and blueSeis-3A, which are a ring laser and a fiber optic gyroscope recording rotational ground motions, all other stations are triaxial broadband seismometers capturing translational ground motions. Blue and green curves denote the train track and highway near the observatory, respectively.

3 Traffic signal classification

The strength and frequencies of traffic-related seismic signals are primarily influenced by engine vibrations, vehicle speeds, and road conditions, generating both Rayleigh and Love waves in the range of approximately 2 to 50 Hz (Nakata, 2016; Díaz et al., 2017; Fuchs and Bokelmann, 2018). Raw particle velocity recordings sampled at 100 Hz from seismometers are corrected for instrument response, detrended, and converted to particle acceleration. The vertical component of continuous acceleration data (Az) from 01:00 a.m. to 02:00 a.m. is presented in Figure 2 for stations TON, FFB2–3, DROMY, and DRMY1–6. We select this midnight period to minimize potential overlaps caused by heavy traffic or other human activities during the day. Notably, similar events are recorded at all stations except TON, which can be attributed to their relative locations and distinct dominant signal sources.

As shown in the site map of Figure 1, all seismic stations, including ROMY, are near the highway, except for station TON, which is closer to the railway. Besides the prominent event around 400 s at station TON, caused by a freight train, we also observe weaker events around 1400 s and 1750 s, likely attributed to commuter trains (Figure 2). To further analyze the signals, we extract two segments of data within the red dashed squares in Figure 2 and present their time-frequency characteristics in Figure 3.

The top panel displays train-related signals recorded at the station pair TON–FFB3, along with their corresponding spectrograms (Figure 3a–b). The arrival time difference of the peak ground motions at two stations is approximately 30 s and can be attributed to the traveling time of the freight train from the nearest point of one station to the other. The waveform amplitude at station FFB3 appears less pronounced than at TON, likely due to rapid attenuation of high-frequency components. However, lower resonance frequencies at FFB3—specifically 5, 9, 12, and 14 Hz—are retained and correspond to those detected at station TON. Furthermore, at TON, there are specific monochromatic spectral lines observed at approximately 16, 26, 37, and 45 Hz. These are thought to be caused by nearby railway electrification and its harmonics (Bormann and Wielandt, 2013; Hu et al., 2018).

The bottom panel of Figure 3 presents car-related signals recorded at stations FFB2 and FFB3. The amplitude and arrival time difference of these signals are less pronounced than those at stations TON and FFB3, likely due to their closer proximity. Common features in the spectrograms shown in Figure 3c–d indicate that both signals originate from the same sources. The lack of higher frequency components (above 20 Hz) at station FFB2, compared to FFB3, is primarily attributed to attenuation, similar to what is observed with the train signals at station FFB3.

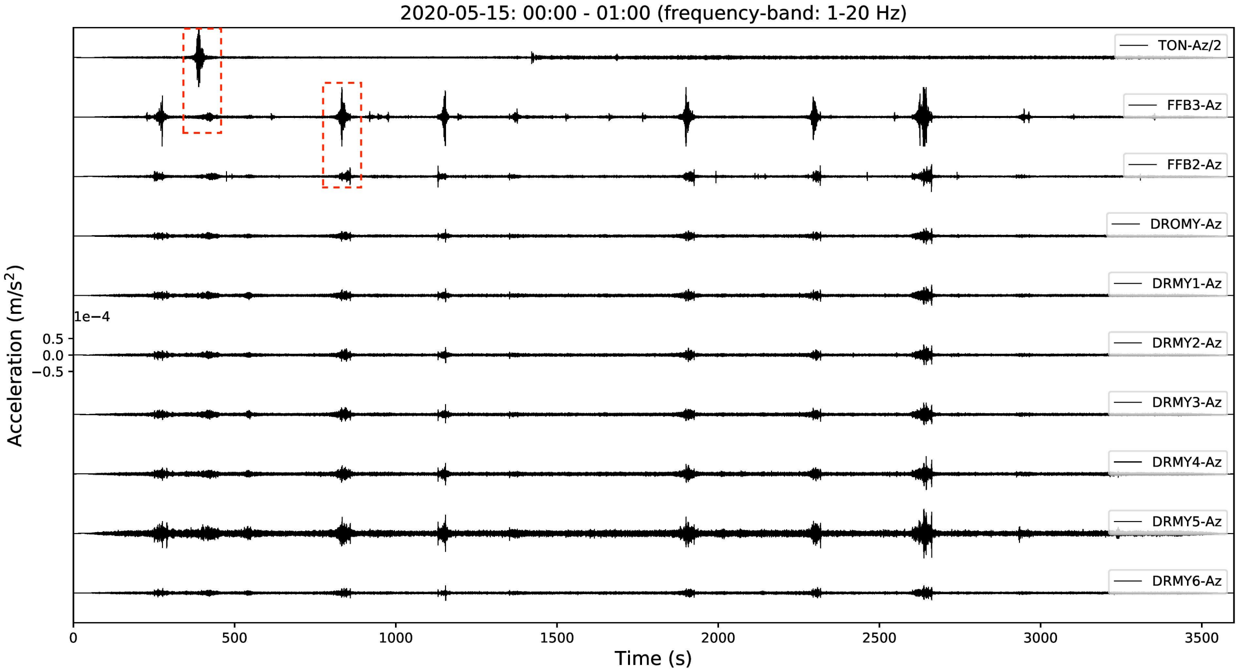

Figure 2: Traffic-induced seismic signals recorded by the seismometers shown in Figure 1 from 1:00 a.m. to 2:00 a.m on May 15, 2020. The vertical component of the raw particle velocity records from the seismometers has been corrected for instrument response, detrended, converted to particle acceleration, and band-pass filtered into 1-20 Hz. All waveforms are plotted to the same scale, except for station TON, where the waveform amplitude has been divided by a factor of 2. The spectrograms for the waveform enclosed by the red dashed square are shown in Figure 3.

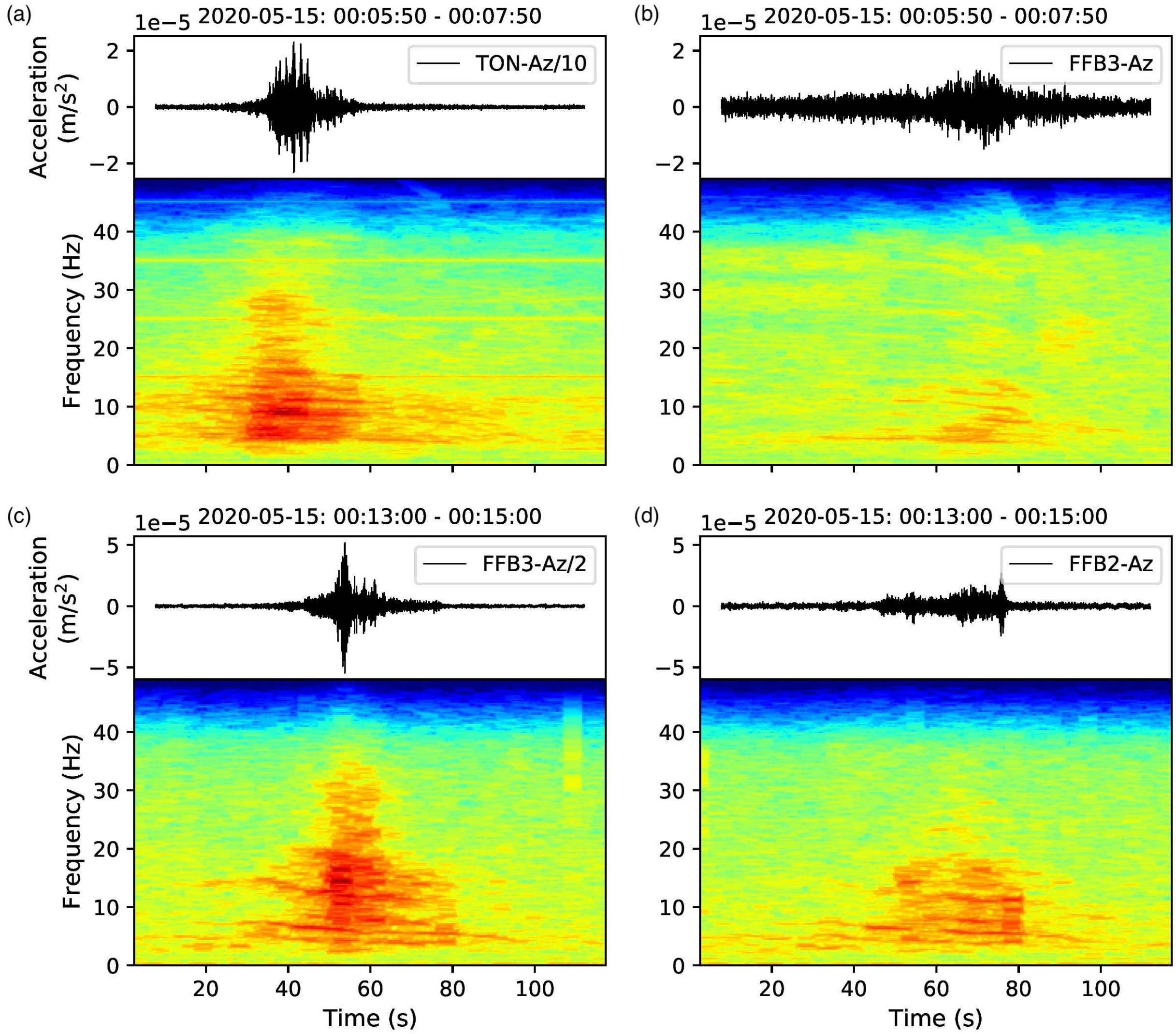

Figure 3: Vertical components of acceleration waveform and spectrograms of the train- (a–b) and car-induced (c–d) seismic signals recorded by the TON, FFB3, and FUR stations. The waveform amplitude at station TON is divided by a scaling factor of 10 in (a) and FFB3 is divided by 2 in (c) for visualization purposes.

4 Tracking vehicle sources using 6C single-station measurement

The capability of 6C single-station measurements in estimating earthquake back-azimuth (Baz) has been demonstrated in several studies (e.g., Igel et al., 2007; Hadziioannou et al., 2012; Yuan et al., 2020a; Chen et al., 2023). The key principle underlying this method is that the rotational sensor acts as a polarization-propagation filter. This filter not only eliminates longitudinal waves but also separates SV- and SH-type ground motions into horizontal and vertical rotational components, respectively.

4.1 6C single-station measurement using Love waves

When focusing on SH and/or Love waves in isotropic medium, we can exclusively analyze the vertical component of rotational motions. The Baz estimation process involves rotating the horizontal translational components through a range of trial Baz values (0° to 360°) to obtain radial and transverse components. We then calculate the zero-lag cross-correlation (CC) coefficient between the transverse acceleration (At) and vertical rotational rate (Rz) for each trial Baz. Assuming that the cross-correlation between Love and Rayleigh waves is significantly smaller than the variance of Rayleigh waves, the CC coefficient reaches its maximum when the trial Baz aligns with the actual Baz, as both represent the same portion of ground motion. Importantly, this 6C approach simultaneously resolves the 180° ambiguity that is a challenge for conventional 3C single-station methods. We apply the CC-based algorithm to the same period of data shown in Figure 2 for the ROMY 6C station, with the results presented in Figure 4a–d. We also analyze a different time period for the BS 6C station, with results shown in Figure 5.

Given the relative position of the 6C stations and the highway (Figure 1), we expect the Baz variations of inbound vehicles (moving from southeast to northwest) to decrease from 100° to 0° and then continue decreasing from 360° to 300°. The patterns for outbound vehicles will be the reverse. Although the ROMY and BS 6C stations collect data from different time periods, the retrieved Baz should exhibit similar patterns of variations due to their relative locations to the highway (Figure 1). Figure 4d and Figure 5c demonstrate the comparable bi-directional variation patterns in the estimated Baz for the ROMY 6C station and the BS station, respectively. For the cross-correlation (CC) analysis, we use a 10-second sliding window for the ROMY station and a 1.5-second sliding window for the BS station. Shorter windows will offer better temporary resolution in resolving faster varying Baz while being potentially more affected by noise levels and overlapping signals for individual windows. We apply 95% overlap for the sliding windows and retain only Baz values with a CC coefficient higher than 0.4 to reduce interference from signals with low signal-to-noise

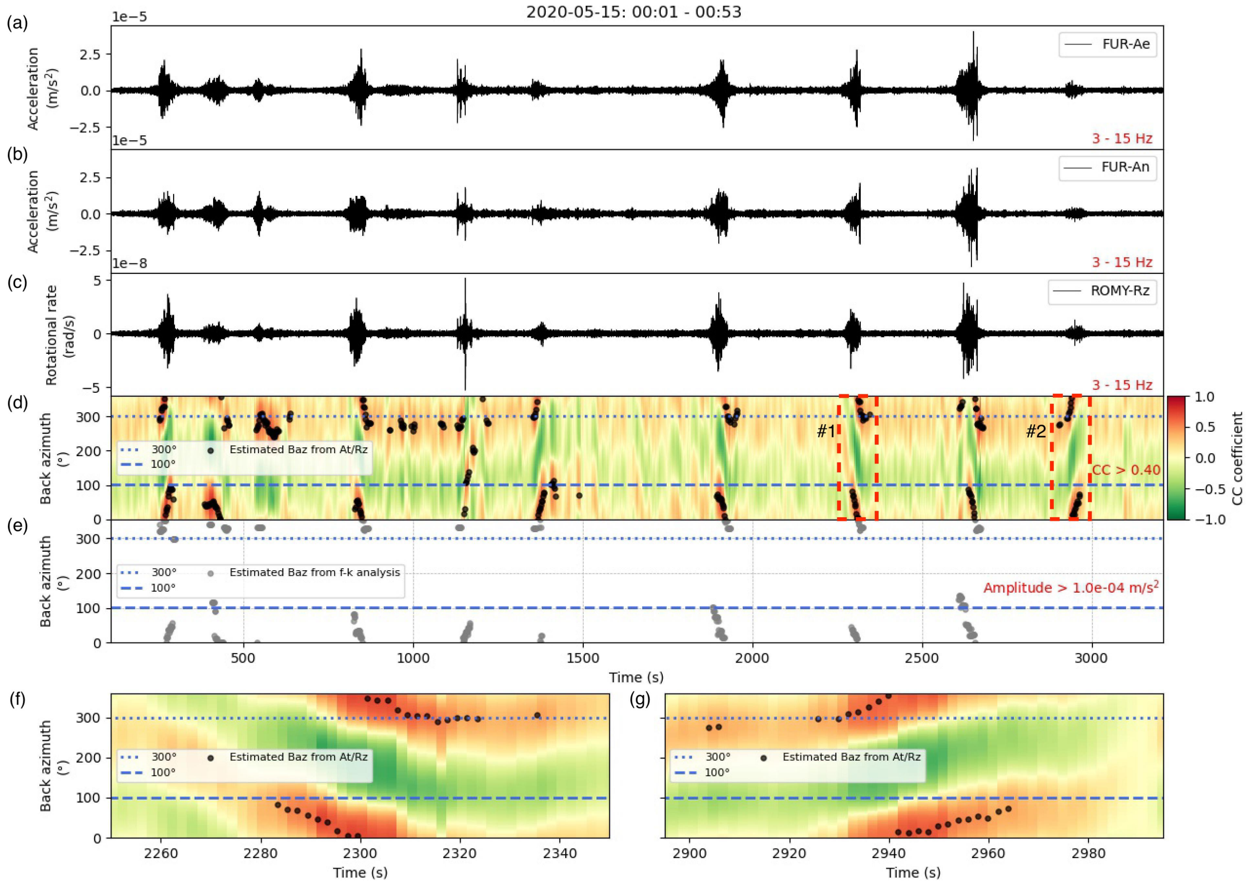

Figure 4: Back azimuth (Baz) estimation of the car-induced Love waves from 6C single-station measurement at station ROMY. The north-south (a) and east-west (b) components of acceleration at FUR station. (c) The vertical rotational rate at ROMY station. (d) Estimated Baz from Ae/An and Rz components using CC method. (e) Estimated Baz from the f-k analysis. The background colors represent CC coefficients and the dots in (c) and (d) denote the estimated Baz for each sliding window with a CC coefficient higher than 0.3 and maximum amplitude larger than 10^{-4} m/s^2, respectively. (f) and (g) correspond to the zoom-in plots within #1 and #2 red squares in (d), respectively.

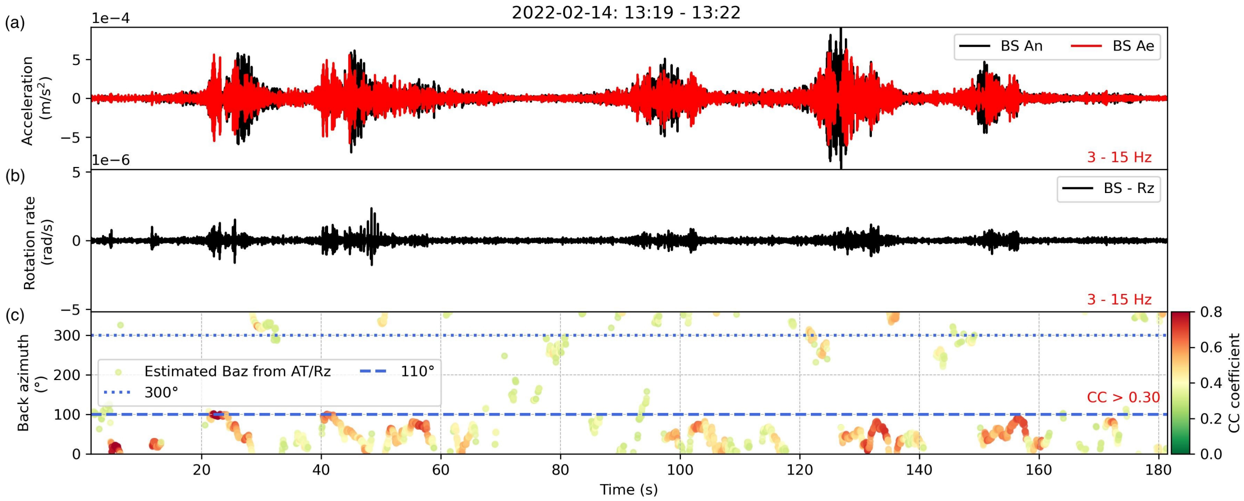

Figure 5: Back azimuth (Baz) estimation of the car-induced Love waves from 6C single-station measurement at station BS. The north-south (a) and east-west (b) components of acceleration at FUR station. (c) The vertical rotational rate at ROMY station. The color of the dots represents the CC coefficients higher than 0.3.

ratios.

From the zoom-in plots of two selected time windows within the red squares in Figure 4d at station ROMY, we can calculate the moving speeds of vehicles through the ratio of distance and time over a certain Baz variation range. The estimated average speed in Figure 4f for the Baz changing from 80° to 0° is approximately 90 km/h and the one in Figure 4g is approximately 65 km/h. Both estimates are considered empirically reasonable for this time of night. The smaller slope of the Baz variation between 0° and 30° is thought to be associated with potential braking operations related to a road exit.

4.2 6C single-station measurement using Rayleigh waves

Our approach goes beyond just using SH-type waves. We also use SV and Rayleigh waves generated by moving vehicles, which can be detected through their horizontal rotational components. This approach is akin to the polarization analysis of P waves with a conventional triaxial seismometer, as P and SH-type waves are not included in the horizontal rotational components. Specifically, we start by conducting a polarization analysis using singular value decomposition (e.g., Gal and Reading, 2019) and then calculate the polarization angle between the two rotational components using the following equation:

$$\theta_{Baz} = -\arctan\left(\frac{\dot{R}_n}{\dot{R}_e}\right), \tag{1}$$

where $\dot{R}_n$ and $\dot{R}_e$ denote the north-south and east-west components of rotational rate, respectively. The θ_{Baz} value derived from the inverse tangent function is between 0° and 180°. To remove the 180° ambiguity, we then compare the rotated transverse component of rotational rate ($\dot{R}_t$) based on θ_{Baz} with the vertical component of acceleration (A_z) through zero-lag CC. If the CC coefficient is positive, 180° should be added to θ_{Baz}.

As the horizontal rotational components of ROMY were under technical maintenance during the period that we deployed the temporal array (DROMY and DRMY1–6), we chose another chunk of data a year ago (from 00:00 a.m.–01:00 a.m., May 15, 2019) as shown in Figure 6a–c. In spite of the date difference, we expect to see similar bi-directional patterns for the Baz estimate due to the generally unchanged road condition. The horizontal rotational motions (Re and Rn) are noisier than acceleration and vertical rotational motions (Rz). The glitches and spurious events in Figure 6c mostly result from mode jumps of the laser due to the unstable cavity length and/or outgassing effect.

The estimated Baz at the ROMY 6C station from Re/Rn and Az components using the polarization method described above is shown in Figure 6e, while that from Ae/An and Rz components using CC method is shown in Figure 6d for comparison. Despite the relatively low signal-to-noise ratios of Re and Rn components, we could still identify consistent Baz variation patterns within certain time windows. When the stability of horizontal rotational components of ROMY gets improved in the future, we expect better agreement.

In contrast to the ROMY station, the horizontal component of the portable rotation sensor at the BS station does not experience instrumental instability. We can clearly observe Baz variations due to moving vehicles (Figure 7c). The retrieved Baz primarily relies on Rayleigh waves since we are using horizontal rotational components. The results are consistent not only with the Baz derived from Love waves at the same station (Figure 5) but also with those obtained from the ROMY station (Figure 6). By comparing the peak amplitudes of the horizontal and vertical components of rotation at the BS station (Figure 5a–b and Figure 7a–b), we can find that the car-induced Rayleigh waves exhibit higher signal-to-noise ratios. This allows for more stable and robust Baz estimation through polarization analysis of the horizontal components of the rotational recordings.

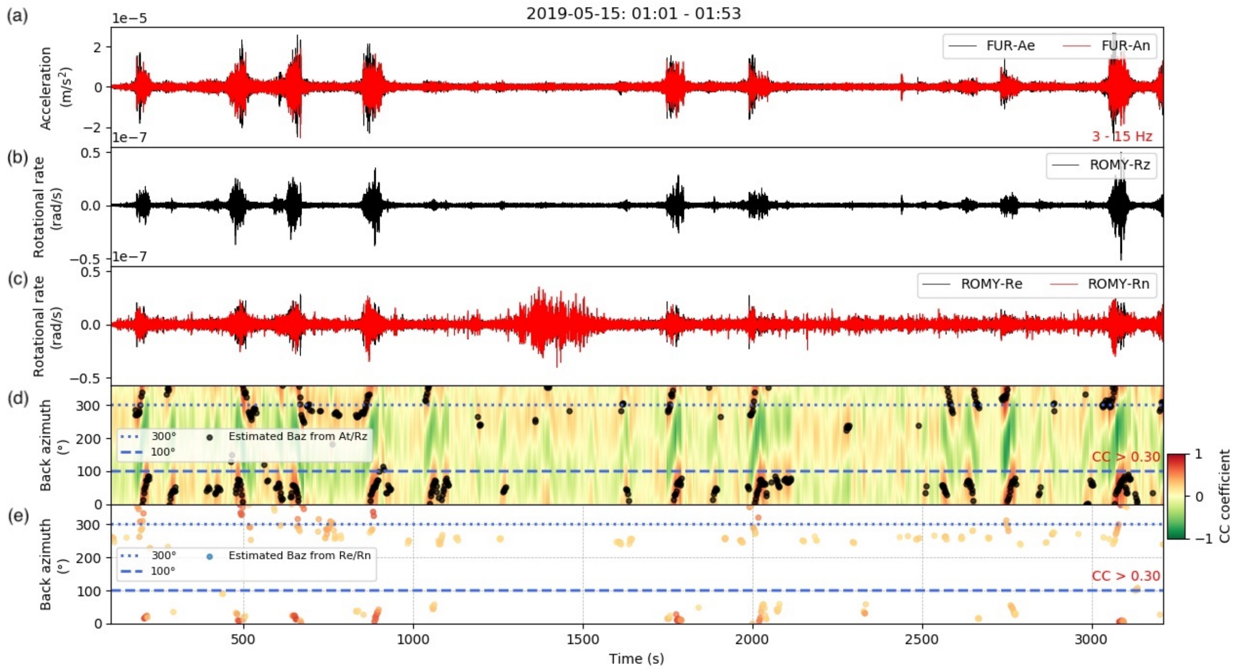

Figure 6: Baz estimation of the car-induced Rayleigh and Love waves from 6C single-station measurement at station ROMY. (a) The north-south (red) and east-west (black) components of acceleration at station FUR. (b) The vertical rotational rate at station ROMY. (c) The north-south (red) and east-west (black) components of rotational rate at station ROMY. The black dashed square represents a spurious event caused by instrumental instability. (d) Estimated Baz from Ae/An and Rz components using CC method focusing on Love waves. (e) Estimated Baz from Re/Rn and Az components using polarization method focusing on Rayleigh waves. The background colors represent CC coefficients and the dots denote the estimated Baz for each sliding window with a CC coefficient higher than 0.3.

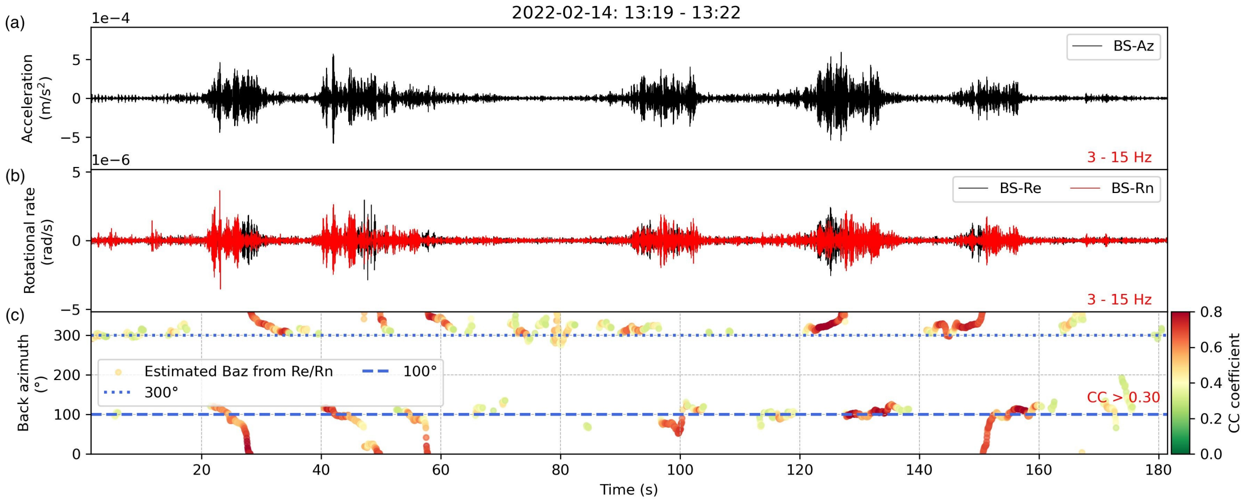

Figure 7: Back azimuth (Baz) estimation of the car-induced Rayleigh waves from 6C single-station measurement at station BS. The north-south (a) and east-west (b) components of acceleration at FUR station. (c) The vertical rotational rate at ROMY station. (d) Estimated Baz from Ae/An and Rz components using CC method. The color of the dots represents the CC coefficients higher than 0.3.

5 Tracking vehicle sources using frequency-wavenumber analysis

A practical way to validate the proposed 6C single-station measurement is to use a seismic array, which can deliver similar information through beamforming. Array-based beamforming or frequency-wavenumber (f-k) analysis is commonly employed for wave-type identification, source direction estimation (i.e., Baz), and slowness estimation of incoming waves. A detailed description of the methodology can be found in Gal and Reading (e.g., 2019). Ideally, we should achieve very similar temporal variations of the seismic source Baz through both array and single-station measurements. Therefore, we deployed a small-scale seismic array (DROMY and DRMY1–6 shown in the zoom-in plot of Figure 1) around the 6C station. Alongside the permanent stations FFB1 and FFB2, we applied f-k analysis to the array data over the same time period to estimate Baz using a consistent sliding window.

In Figure 4e, we exclude samples of the estimated Baz with a maximum amplitude smaller than $1.0e^{-4}$ m/s^2 within the corresponding time window. There is a strong agreement between the Baz variations obtained from the 6C measurement (Figure 4d) and the f-k analysis (Figure 4e). The difference between Figure 4d and 4e can be mainly attributed to three factors. First, the array-based f-k analysis relies on SV/Rayleigh waves, as it uses the vertical components of acceleration, while the 6C single-station analysis is based on SH/Love waves. The radiation patterns of these different wave types may vary, resulting in unequal signal-to-noise ratios within the same time window. Second, we filter the estimated Baz using the cross-correlation coefficient for the 6C analysis, whereas in the f-k analysis, we apply an amplitude threshold. Third, the geometry of the array affects the resolution capabilities of the f-k analysis, which may also contribute to discrepancies between the two measurement methods. These factors combined may explain the differences observed when comparing the f-k and 6C single-station measurements.

6 Tracking vehicle sources using array-derived rotation

Rotational motions can essentially be represented by spatial gradients of translational motions, allowing us to calculate them indirectly using closely spaced triaxial seismometers (e.g., Spudich et al., 1995). This approach is known as array-derived rotation (ADR). Despite its band-limited accuracy (Langston, 2007), ADR provides an independent way to validate rotational motions recorded directly by rotational sensors. To verify the proposed 6C single-station measurement, we first compute the three components of ADR for the reference station DROMY using data from the surrounding stations DRMY1–3 (Figure 8b–c). We then apply the same processing strategy outlined in Section 4 to both the ADR and acceleration records at station DROMY. As shown in Figure 8d–e, the estimated Baz variations from SH/Love waves (At/Rz) and SV/Rayleigh waves (Rz/Rt) are not only consistent with each other, but also align well with those obtained from the 6C single-station measurement at stations ROMY and BS.

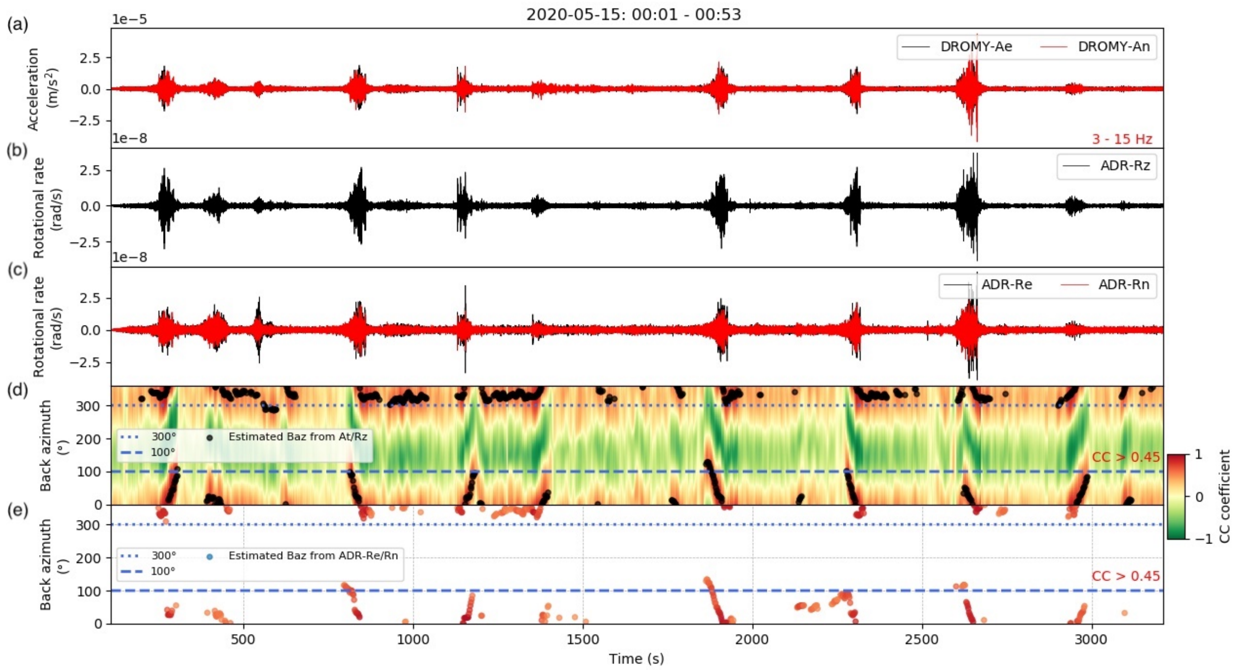

Figure 8: 6C measurement applied onto array-derived rotation (ADR). (a) The north-south (red) and east-west (black) components of acceleration at DROMY station. (b) The vertical component of array-derived rotational rate at DROMY station. (c) The north-south (red) and east-west (black) components of array-derived rotational rate at DROMY station. (d) Estimated Baz from Ae/An and array-derived Rz using CC method focusing on Love waves. (e) Estimated Baz from array-derived Re/Rn and Az components using polarization method focusing on Rayleigh waves. The background colors represent CC coefficients and the dots denote the estimated Baz for each sliding window with a CC coefficient higher than 0.45.

7 Discussion

Although this study concentrates on traffic signals, the 6C measurements have the potential for wide applicability to various seismic sources in both urban and natural environments. The seismic source we refer here is to any source that can generate ground vibrations that seismometers can detect. Analyzing these diverse source distributions could enhance our understanding of natural processes such as river sediment transportation and bedrock erosion (Burtin et al., 2010), Earth-ocean-atmosphere interactions (Kedar and Webb, 2005). It could also provide insights into geological phenomena including volcanic activities (Brenguier et al., 2011; Obermann et al., 2013) and earthquakes (Hadziioannou et al., 2011; Obermann et al., 2014). Furthermore, this technique shows promise for monitoring natural hazards like landslides (Suriñach Cornet et al., 2005; Tonnellier et al., 2013) and hurricanes (Davy et al., 2014; Fan et al., 2019). The rotational components of 6C measurements naturally separate Rayleigh and Love waves, potentially enhancing detection, classification, and monitoring of diverse seismic events based on their time and frequency characteristics.

Ground vibrations from various sources provide valuable data for inferring near-surface structures. By determining the directionalities of both static and dynamic sources, we effectively transform passive seismic experiments into active ones. Moving objects, such as vehicles, can be considered as moving impulse sources that continuously generate ground shaking with varying azimuth and distance. Recent studies have shown that 6C measurements can extract surface wave dispersion characteristics and invert for shear-wave profiles (e.g., Wassermann et al., 2016; Keil et al., 2021). The continuous nature of many anthropogenic and natural sources allows for potential monitoring of dynamic changes in subsurface structures over time, complementing conventional active and passive techniques, especially in complex geological and urban settings.

Traditional three-component single seismic station can be used to estimate attenuation parameters from traffic noise, which is crucial for near-surface characterization (Zhao et al., 2023). With a 3C single seismometer, the attenuation model is often simplified as frequency-independent, a useful approximation particularly at low frequencies. However, using the proposed 6C method, which naturally separates wave types and retrieves dispersion information from both Rayleigh and Love waves (Yuan et al., 2020b), we can potentially implement a frequency-dependent attenuation model. This model may better capture the complexities of the near-surface, especially at higher frequencies where traffic noise becomes a significant factor.

Although the two types of rotational seismometers are among the most sensitive options available, they come at a higher cost compared to standard broadband seismometers (Bernauer et al., 2018; Yuan et al., 2020b). The ring laser gyroscope, in particular, is too bulky and expensive for seismological field observations

(Igel et al., 2021). Typically, the cost of rotational sensors is proportional to their sensitivity and frequency range. However, in many urban and environmental applications, target signals are band-limited and possess higher energy levels than those observed in traditional earthquake studies. This presents an opportunity to develop specific, cost-effective portable rotational instruments using fiber-optic or alternative measurement principles (Brokešová and Málek, 2013).

8 Conclusions

We show that the joint analysis of collocated translational and rotational ground motions can be used to track moving vehicles. This array-like functionality of the 6C single-station measurement makes it appealing especially when seismic arrays are difficult to deploy because of unfavorable environments, such as ocean bottom, mountainous area, and planetary objects.

As a single-station measurement technique, 6C analysis offers a flexible alternative to conventional array measurements for separating wavefield components, estimating source directionality, and characterizing near-surface structures (Edme and Yuan, 2016; Wassermann et al., 2016). This approach opens up new possibilities in seismology, particularly in challenging environments and for continuous monitoring applications. The versatility and potential of 6C measurements suggest that they could play a significant role in advancing our understanding of various Earth processes and in developing more effective monitoring systems for both natural events and anthropogenic activities.

Data and resources

The datasets used in this study are available at the following GitHub repository: https://github.com/Shihao-Yuan/6C-source-tracking. The software toolbox ObsPy (Megies et al., 2011) was used for data processing.

Acknowledgments

This research is partially supported by the European Research Council (ROMY project, Grant No. 339991), the National Science Foundation (Award No. 2046387), and the U.S. Geological Survey Earthquake Hazards Program (Grant No. G24AS00292).

References

Almendros, J., Ibáñez, J. M., Alguacil, G., and Del Pezzo, E. (1999). Array analysis using circular-wave-front geometry: An application to locate the nearby seismo-volcanic source. *Geophysical Journal International*, 136(1):159–170.

Asgari, S., Stafsudd, J. Z., Hudson, R. E., Yao, K., and Taciroglu, E. (2015). Moving source localization using seismic signal processing. *Journal of Sound and Vibration*, 335:384–396.

Bernauer, F., Wassermann, J., Guattari, F., Frenois, A., Bigueur, A., Gaillot, A., de Toldi, E., Ponceau, D., Schreiber, U., and Igel, H. (2018). Blueseis3a: Full characterization of a 3C broadband rotational seismometer. *Seismological Research Letters*, 89(2A):620–629.

Bormann, P. and Wielandt, E. (2013). Seismic signals and noise. In *New Manual of Seismological Observatory Practice 2 (NMSOP2)*, pages 1–62. Deutsches GeoForschungsZentrum GFZ.

Brenguier, F., Clarke, D., Aoki, Y., Shapiro, N. M., Campillo, M., and Ferrazzini, V. (2011). Monitoring volcanoes using seismic noise correlations. *Comptes Rendus Geoscience*, 343(8-9):633–638.

Brokešová, J. and Málek, J. (2013). Rotaphone, a self-calibrated six-degree-of-freedom seismic sensor and its strong-motion records. *Seismological Research Letters*, 84(5):737–744.

Burtin, A., Vergne, J., Rivera, L., and Dubernet, P. (2010). Location of river-induced seismic signal from noise correlation functions. *Geophysical Journal International*, 182(3):1161–1173.

Chen, C., Wang, Y., Sun, L., Lin, C.-J., Wei, Y., Liao, C., Lin, B., and Qin, L. (2023). Six-component earthquake synchronous observations across Taiwan strait: Phase velocity and source location. *Earth and Space Science*, 10(12):e2023EA003040.

Davy, C., Barruol, G., Fontaine, F. R., Sigloch, K., and Stutzmann, E. (2014). Tracking major storms from microseismic and hydroacoustic observations on the seafloor. *Geophysical Research Letters*, 41(24):8825–8831.

Díaz, J., Ruiz, M., Sánchez-Pastor, P. S., and Romero, P. (2017). Urban seismology: On the origin of earth vibrations within a city. *Scientific reports*, 7(1):1–11.

Diaz, J., Ruiz, M., Udina, M., Polls, F., Martí, D., and Bech, J. (2023). Monitoring storm evolution using a high-density seismic network. *Scientific reports*, 13(1):1853.

Edme, P. and Yuan, S. (2016). Local dispersion curve estimation from seismic ambient noise using spatial gradients. *Interpretation*, 4(3):SJ17–SJ27.

Fan, W., McGuire, J. J., de Groot-Hedlin, C. D., Hedlin, M. A., Coats, S., and Fiedler, J. W. (2019). Stormquakes. *Geophysical Research Letters*, 46(22):12909–12918.

Fuchs, F. and Bokelmann, G. (2018). Equidistant spectral lines in train vibrations. *Seismological Research Letters*, 89(1):56–66.

Gal, M. and Reading, A. M. (2019). Beamforming and polarization analysis. *Seismic Ambient Noise*, page 30.

Gebauer, A., Tercjak, M., Schreiber, K. U., Igel, H., Kodet, J., Hugentobler, U., Wassermann, J., Bernauer, F., Lin, C.-J., Donner, S., et al. (2020). Reconstruction of the instantaneous earth rotation vector with sub-arcsecond resolution using a large scale ring laser array. *Physical Review Letters*, 125(3):033605.

Greenhalgh, S., Sollberger, D., Schmelzbach, C., and Rutty, M. (2018). Single-station polarization analysis applied to seismic wavefields: A tutorial. *Advances in Geophysics*, 59:123–170.

Hadziioannou, C., Gaebler, P., Schreiber, U., Wassermann, J., and Igel, H. (2012). Examining ambient noise using colocated measurements of rotational and translational motion. *Journal of seismology*, 16(4):787–796.

Hadziioannou, C., Larose, E., Baig, A., Roux, P., and Campillo, M. (2011). Improving temporal resolution in ambient noise monitoring of seismic wave speed. *Journal of Geophysical Research: Solid Earth*, 116(B7).

Heck, M., Hobiger, M., Van Herwijnen, A., Schweizer, J., and Fäh, D. (2019). Localization of seismic events produced by avalanches using multiple signal classification. *Geophysical Journal International*, 216(1):201–217.

Hu, H., Shao, Y., Tang, L., Ma, J., He, Z., and Gao, S. (2018). Overview of harmonic and resonance in railway electrification systems. *IEEE Transactions on Industry Applications*, 54(5):5227–5245.

Igel, H., Cochard, A., Wassermann, J., Flaws, A., Schreiber, U., Velikoseltsev, A., and Pham Dinh, N. (2007). Broad-band observations of earthquake-induced rotational ground motions. *Geophysical Journal International*, 168(1):182–196.

Igel, H., Schreiber, K. U., Gebauer, A., Bernauer, F., Egdorf, S., Simonelli, A., Liny, C.-J., Wassermann, J., Donner, S., Hadziioannou, C., Yuan, S., Brotzer, A., Kodet, J., Tanimoto, T., Hugentobler, U., and Wells7, J.-P. R. (2021). ROMY: A Multi-Component Ring Laser for Geodesy and Geophysics. *Geophysical Journal International*. ggaa614.

Kedar, S. and Webb, F. H. (2005). The ocean's seismic hum. *Science*, 307(5710):682–683.

Keil, S., Wassermann, J., and Igel, H. (2021). Single-station seismic microzonation using 6C measurements. *Journal of Seismology*, 25:103–114.

Krim, H. and Viberg, M. (1996). Two decades of array signal processing research: the parametric approach. *IEEE signal processing magazine*, 13(4):67–94.

Langston, C. A. (2007). Spatial gradient analysis for linear seismic arrays. *Bulletin of the Seismological Society of America*, 97(1B):265–280.

Lindsey, N. J. and Martin, E. R. (2021). Fiber-optic seismology. *Annual Review of Earth and Planetary Sciences*, 49(1):309–336.

Liu, H., Ma, J., Xu, T., Yan, W., Ma, L., and Zhang, X. (2019). Vehicle detection and classification using distributed fiber optic acoustic sensing. *IEEE Transactions on Vehicular Technology*, 69(2):1363–1374.

Manconi, A., Picozzi, M., Coviello, V., De Santis, F., and Elia, L. (2016). Real-time detection, location, and characterization of rockslides using broadband regional seismic networks. *Geophysical Research Letters*, 43(13):6960–6967.

Martin, E., Lindsey, N., Dou, S., Ajo-Franklin, J., Daley, T., Freifeld, B., Robertson, M., Ulrich, C., Wagner, A., and Bjella, K. (2016). Interferometry of a roadside DAS array in Fairbanks, AK. In *SEG Technical Program Expanded*

Abstracts 2016, pages 2725–2729. Society of Exploration Geophysicists.

Megies, T., Beyreuther, M., Barsch, R., Krischer, L., and Wassermann, J. (2011). ObsPy–what can it do for data centers and observatories? *Annals of Geophysics*, 54(1):47–58.

Nakata, N. (2016). Near-surface S-wave velocities estimated from traffic-induced love waves using seismic interferometry with double beamforming. *Interpretation*, 4(4):SQ23–SQ31.

Obermann, A., Froment, B., Campillo, M., Larose, E., Planes, T., Valette, B., Chen, J., and Liu, Q. (2014). Seismic noise correlations to image structural and mechanical changes associated with the mw 7.9 2008 wenchuan earthquake. *Journal of Geophysical Research: Solid Earth*, 119(4):3155–3168.

Obermann, A., Planes, T., Larose, E., and Campillo, M. (2013). Imaging preeruptive and coeruptive structural and mechanical changes of a volcano with ambient seismic noise. *Journal of Geophysical Research: Solid Earth*, 118(12):6285–6294.

Reinwald, M., Moseley, B., Szenicer, A., Nissen-Meyer, T., Oduor, S., Vollrath, F., Markham, A., and Mortimer, B. (2021). Seismic localization of elephant rumbles as a monitoring approach. *Journal of the Royal Society Interface*, 18(180):20210264.

Riahi, N. and Gerstoft, P. (2015). The seismic traffic footprint: Tracking trains, aircraft, and cars seismically. *Geophysical Research Letters*, 42(8):2674–2681.

Spudich, P., Steck, L. K., Hellweg, M., Fletcher, J., and Baker, L. M. (1995). Transient stresses at parkfield, california, produced by the m 7.4 landers earthquake of june 28, 1992: Observations from the upsar dense seismograph array. *Journal of Geophysical Research: Solid Earth*, 100(B1):675–690.

Suriñach Cornet, E., Vilajosana Guillén, I., Khazaradze, G., Biescas Górriz, B., Furdada i Bellavista, G., and Vilaplana, J. M. (2005). Seismic detection and characterization of landslides and other mass movements. *Natural Hazards and Earth System Sciences, 2005, Vol. 5, p. 791-798.*

Tape, C., Ringler, A. T., and Hampton, D. L. (2020). Recording the aurora at seismometers across Alaska. *Seismological Research Letters*, 91(6):3039–3053.

Tonnellier, A., Helmstetter, A., Malet, J.-P., Schmittbuhl, J., Corsini, A., and Joswig, M. (2013). Seismic monitoring of soft-rock landslides: the Super-Sauze and Valoria case studies. *Geophysical Journal International*, 193(3):1515–1536.

Venkatraman, D., Reddy, V., and Khong, A. W. (2011). A study of the ambiguity problem in footstep bearing estimation using tri-axial geophone. In *2011 8th International Conference on Information, Communications & Signal Processing*, pages 1–5. IEEE.

Wang, H., Quan, W., Wang, Y., and Miller, G. R. (2014). Dual roadside seismic sensor for moving road vehicle detection and characterization. *Sensors*, 14(2):2892–2910.

Wassermann, J., Wietek, A., Hadziioannou, C., and Igel, H. (2016). Toward a single-station approach for microzonation: Using vertical rotation rate to estimate love-wave dispersion curves and direction finding. *Bulletin of the Seismological Society of America*, 106(3):1316–1330.

Yuan, S., Gessele, K., Gabriel, A.-A., May, D. A., Wassermann, J., and Igel, H. (2020a). Seismic source tracking with six degree-of-freedom ground motion observations. *Journal of Geophysical Research: Solid Earth*, page e2020JB021112.

Yuan, S., Simonelli, A., Lin, C.-J., Bernauer, F., Donner, S., Braun, T., Wassermann, J., and Igel, H. (2020b). Six degree-of-freedom broadband ground-motion observations with portable sensors: Validation, local earthquakes, and signal processing. *Bulletin of the Seismological Society of America*, 110(3):953–969.

Zhao, Y., Nilot, E. A., Li, B., Fang, G., Luo, W., and Li, Y. E. (2023). Seismic attenuation extraction from traffic signals recorded by a single seismic station. *Geophysical Research Letters*, 50(3):e2022GL100548.